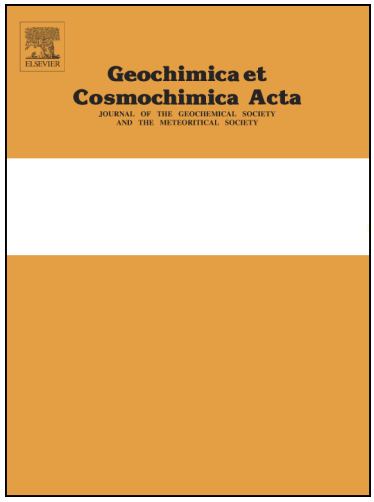

Sedimentary pyrite δ ^{34}S differs from porewater sulfide in Santa Barbara Basin: proposed role of organic sulfur

Morgan Reed Raven, Alex L. Sessions, Woodward W. Fischer, Jess F. Adkins

PII: S0016-7037(16)30206-X
DOI: http://dx.doi.org/10.1016/j.gca.2016.04.037
Reference: GCA 9732

To appear in: *Geochimica et Cosmochimica Acta*

Received Date: 10 June 2015
Accepted Date: 19 April 2016

Please cite this article as: Raven, M.R., Sessions, A.L., Fischer, W.W., Adkins, J.F., Sedimentary pyrite δ ^{34}S differs from porewater sulfide in Santa Barbara Basin: proposed role of organic sulfur, *Geochimica et Cosmochimica Acta* (2016), doi: http://dx.doi.org/10.1016/j.gca.2016.04.037

Sedimentary pyrite $\delta^{34}S$ differs from porewater sulfide in Santa Barbara Basin: proposed role of organic sulfur

Morgan Reed Raven [a*], Alex L. Sessions [a], Woodward W. Fischer [a], Jess F. Adkins [a]

[a] *Division of Geological and Planetary Sciences, California Institute of Technology, Pasadena, CA 91125, USA*

** corresponding author: mrraven@caltech.edu, (626) 395-8647*

Abstract

Santa Barbara Basin sediments host a complex network of abiotic and metabolic chemical reactions that knit together the carbon, sulfur, and iron cycles. From a 2.1-m sediment core collected in the center of the basin, we present high-resolution profiles of the concentrations and isotopic compositions of all the major species in this system: sulfate, sulfide ($\sum H_2S$), elemental sulfur (S^0), pyrite, extractable organic sulfur (OS), proto-kerogen S, total organic and dissolved inorganic carbon, and total and reducible iron. Below 10 cm depth, the core is characterized by low apparent sulfate reduction rates (<0.01 mM/yr) except near the sulfate-methane transition zone. Surprisingly, pyrite forming in shallow sediments is ~30‰ more ^{34}S-depleted than coexisting $\sum H_2S$ in porewater. S^0 has the same strongly ^{34}S-depleted composition as pyrite where it forms near the sediment–water interface, though not at depth. This pattern is not easily explained by conventional hypotheses in which sedimentary pyrite derives from abiotic reactions with porewater $\sum H_2S$ or from the products of S^0 disproportionation. Instead, we propose that pyrite formation in this environment occurs within sulfate reducing microbial aggregates or biofilms, where it reflects the isotopic composition of the immediate products of bacterial sulfate reduction. Porewater $\sum H_2S$ in Santa Barbara Basin may be more ^{34}S-enriched than pyrite due to equilibration with relatively ^{34}S-enriched OS. The difference between OS and pyrite $\delta^{34}S$ values would then reflect the

balance between microbial sulfide formation and the abundance of exchangeable OS. Both OS and pyrite $\delta^{34}S$ records thus have the potential to provide valuable information about biogeochemical cycles and redox structure in sedimentary paleoenvironments.

1. Introduction

Pyrite burial in sediments represents one of the largest fluxes in the global sulfur cycle (Bottrell and Newton, 2006). Records of the sulfur-isotopic composition of sedimentary pyrite have informed studies of the evolution of major metabolic pathways (Canfield and Teske, 1996; Bontognali et al., 2013), the size of the marine sulfate reservoir (Habicht et al., 2002; Canfield, 2004), and the redox balance of the planet (Berner and Raiswell, 1983; Leavitt et al., 2013). In these applications, pyrite $\delta^{34}S$ is typically assumed to record the sulfur isotopic composition of porewater sulfide ($\sum H_2S$) (e.g., Anderson and Pratt, 1995; Johnston et al., 2005; Leavitt et al., 2013). Nevertheless, we have only a partial understanding of the microbial and abiotic processes affecting the $\delta^{34}S$ values of pyrite, $\sum H_2S$, and other sedimentary sulfur pools in modern environments.

Pyrite is the product of one of two reactions that involve sulfide either directly (as S^{2-}) or indirectly (via polysulfides).

$$Fe^{2+} + HS^- \rightarrow [FeS] + H^+ \qquad (1) \qquad \text{(rapid)}$$

$$[FeS] + S_n^{2-} \rightarrow FeS_2 + S_{(n-1)}^{2-} \qquad (2a)$$

$$[FeS] + H_2S \rightarrow FeS_2 + H_2 \qquad (2b)$$

Both reactions have been demonstrated experimentally (Butler et al., 2004), and their relative importance depends on pH and the details of polysulfide speciation in any particular environment. In either case, however, pyrite takes on the sulfur-isotope composition of its source with less than 1‰ fractionation (Wilkin and Barnes, 1996; Bottcher et al., 1998; Butler et al., 2004). In the following discussion, we refer to that source as '$\sum H_2S$', which can also be thought of as total inorganic S(-II).

Microbial sulfate reduction (MSR) is the dominant mechanism of organic matter remineralization and sulfide production in anoxic marine sediments (Froelich et al., 1979; Jorgensen, 1982; Bottrell and Newton, 2006). For over three decades it was thought that fractionations associated with MSR (ε_{MSR}) did not exceed 48‰ (Rees, 1973; Goldhaber and Kaplan, 1975; Fry et al., 1991; Detmers et al., 2001). It has since been established that MSR alone is capable of generating large fractionations of >70‰ (Brunner and Bernasconi, 2005; Johnston et al., 2007; Canfield et al., 2010; Sim et al., 2011). Still, there are large discrepancies between experimentally measured MSR fractionation factors for natural microbial communities and the $\delta^{34}S$ values of pyrite from the same environment (Habicht and Canfield, 2001), highlighting our limited understanding of the complexity of the sulfur cycle in many natural systems.

In modern marine sediments, the vast majority of $\sum H_2S$ produced by MSR can be reoxidized (Jorgensen, 1982; Canfield, 1989; Brüchert et al., 2000) both biotically and abiotically by a variety of potential electron acceptors, including oxygen, nitrate, and ferric iron (Canfield, 2001). These reactions produce S^0 and other sulfur intermediates

that are slightly more ^{34}S-depleted than the initial $\sum H_2S$ (Poser et al., 2014), and subsequent disproportionation of these intermediate compounds could generate very strongly ^{34}S-depleted $\sum H_2S$ (Kaplan and Rittenberg, 1964; Fry et al., 1986). The combination of MSR, $\sum H_2S$ oxidation and disproportionation has been hypothesized to drive the $\delta^{34}S$ difference between $\sum H_2S$ and pyrite to exceed the fractionation from MSR (Canfield and Thamdrup, 1994). Moreover, the distribution of ^{34}S in sediments can be influenced by other microbial and abiological reactions, including organic matter sulfurization (Sinninghe Damste et al., 1989; Bruchert et al., 2000), isotopic exchange between different pools (Dale et al., 2009), and enhanced biogeochemical cycling associated with the sulfate-methane transition zone (SMTZ).

To evaluate *in situ* biogeochemical cycling and help constrain how marine sediments acquire and modify their sulfur isotope signatures through organic diagenesis, we collected new sediment cores from the center of the Santa Barbara Basin and measured the major S, C, and Fe pools with very high (2.5-cm) stratigraphic resolution. We employed a new approach to measure $\delta^{34}S$ values of very small samples by multicollector inductively-coupled plasma mass spectrometry (ICP-MS) (Paris et al., 2013). This technique enabled high-resolution depth profiles of both major and minor sulfur species throughout a 2.1-m-long core. We find that the sulfur isotopic composition of porewater $\sum H_2S$ is remarkably different from that of both pyrite and S^0, challenging conventional explanations for their formation. These $\delta^{34}S$ records constrain the possible sources of pyrite sulfur and porewater $\sum H_2S$ and provide new insights into the biogeochemical processes operating in these anoxic sediments.

2. Methods

2.1 Site Background

Sediment cores were taken from the deepest point (~590 m) of Santa Barbara Basin, a silled basin off the coast of southern California that has been extensively studied to take advantage of its high sedimentation rate and annual varves (Soutar and Crill, 1977; Reimers et al., 1990; Schimmelmann et al., 1990; Schimmelmann et al., 2013). Bottom water O_2 concentrations are typically low (<0.1 mL/L; <10 µM) at depths below the western sill of the basin (475 m) except during spring inflow events (Sholkovitz, 1973; Reimers et al., 1996; Moffitt et al., 2014). Sediments in the basin are rich in organic matter and contain up to 4% TOC (Schimmelmann and Kastner, 1993). Shallow sediments are characterized by a dynamic sulfur cycle driven by communities of microorganisms, including both extensive microbial sulfate reduction (MSR) and $\sum H_2S$ reoxidation by widespread *Beggiatoa* mats at the sediment-water interface (Schimmelmann and Kastner, 1993; Kuwabara et al., 1999).

Santa Barbara Basin sediments overlie hydrocarbon-rich sedimentary bedrock that releases methane and other light hydrocarbons. Both thermogenic and biogenic methane may diffuse upward to the sulfate methane transition zone (SMTZ), where enough sulfate is available to drive anaerobic oxidation of methane (AOM). The depth of the SMTZ in Santa Barbara Basin has been reported at as little as 15 cm in seep-type environments (Orphan et al., 2001) and at 120-150 cm in non-seep environments (Berelson et al., 2005; Harrison et al., 2009; Li et al., 2009).

2.2 Porewater Sample Collection

Santa Barbara Basin cores were collected in early October 2013 as part of *R/V Atlantis* cruise AT26-06. Triplicate multicores ('M', 'R', and 'A') and a longer gravity core were collected from approximately the same location in the basin on consecutive days. Immediately after collection, multicore 'M' and the gravity core were extruded and sliced into 2.5-cm-thick discs. Solids were isolated by squeezing in a benchtop, N_2-flushed apparatus (after Reeburgh, 1967) and immediately frozen at -40°C. Porewater was also collected at 2-cm resolution using Rhizon samplers (Rhizosphere Research Products) in multicore 'R' in a 2°C cold room. Porewater aliquots from both the gravity core and multicore 'R' were aliquotted via disposable syringe into vials for sulfate, sulfide, and DIC analyses. Sulfate vials were acidified with high-purity Seastar HCl to volatilize dissolved sulfide. Sulfide vials contained 1 M zinc acetate to trap sulfide as solid ZnS, and an untreated aliquot without headspace was retained for DIC. All porewater samples were stored frozen (-40°C) until analysis. DIC concentrations and $\delta^{13}C$ values were measured by combustion elemental analyzer – isotope ratio mass spectrometry (EA-IRMS, Costech EA, Thermo Delta V+ with Gasbench II) and have estimated uncertainties of ~2% and 0.21‰ (1σ), respectively. Zinc sulfides were washed with milli-Q water and oxidized to sulfate with hydrogen peroxide (90°C, 24 hrs). Porewater sulfate and sulfide were analyzed as sulfate by ICP-MS (see below).

The multi-core preserved the sediment-water interface; the gravity core did not. Initial field observations of the gravity core suggested overpenetration of ~35 cm. Our revised

estimate of ~13 cm overpenetration is based on the linear extrapolation of DIC and sulfate concentrations to seawater values at the sediment-water interface. We also present data from one box core sample (0–10 cm) that was collected at approximately the same location on a prior cruise to Santa Barbara Basin in 2004, as described in Li et al. (2009). This material was frozen without squeezing in heavy-duty Ziploc bags at –40°C until sub-sampling.

2.3 Sample Preparation and Sulfur Analyses

Sediment samples were freeze-dried and then subjected to sequential organic and acid extractions (Fig. 1). Sediments were first microwave-extracted twice with 9:1 dichloromethane (DCM):methanol (MeOH) at 100°C for 15 minutes (MARS 5, CEM Corp). The total lipid extract was separated into fractions by silica gel chromatography, eluting with 4:1 hexane:DCM for non-polar OS, DCM for intermediate-polarity OS (not discussed further here), and 1:1 DCM:MeOH for polar OS. S^0 represents the vast majority of the sulfur in the non-polar extractable organic fraction. A split of this fraction was treated with activated elemental Cu to remove S^0 (Blumer, 1957) and account for the small quantity of non-polar organosulfur compounds in this fraction. Aliquots of the polar OS and treated and untreated non-polar OS fractions were dried and then oxidized in 30% H_2O_2 at 90° C for 24 hours. Solvent-extracted sediments were washed twice with Milli-Q water to remove any residual porewater sulfate and then leached in 1 N nitric acid for 12 days at room temperature to oxidize mineral sulfides, predominantly pyrite, to sulfate (Schimmelmann and Kastner, 1993). This ‘pyrite’ fraction may include a minor amount of other metal disulfides and oxidizable, non-solvent-extractable organosulfur

compounds, but not acid-volatile components, including most mineral monosulfides (Rickard and Morse, 2005). Leached sediments were washed twice with 0.5 N HCl and freeze-dried for residual organic matter analysis.

Oxidized pyrite, S^0, and extractable OS fractions were then purified on AG1-X8 anionic exchange resin (Paris et al., 2013). Resin was washed with ten column volumes (CV) 10% HNO_3, conditioned with 10 CV 10% HCl and 10 CV 0.5% HCl, loaded in trace HCl, and washed with 3x5 CV MQ H_2O before sulfate was eluted in 0.5N HNO_3. Sulfate samples were stored dry in Teflon vials until analysis.

Pyrite, S^0, extractable OS fractions, sulfate and porewater sulfide were quantified as sulfate by ion chromatography (IC, Dionex ICS-2000) with an AS-19 anion column and AERS 500 ion regeneration. The reproducibility of IC concentration measurements was better than 2% (1σ), and external standard replicates, reflecting sample purification, workup, and analysis, had a long-term error of ±10% relative. Concentrations were used to intensity-match samples and the required Na^+ supplement for analysis by inductively coupled plasma – mass spectrometry (ICP-MS, Thermo Neptune$^+$) (Paris et al., 2013). Samples were injected into the plasma torch with a desolvating nebulizer (Aridus) and bracketed with a $NaSO_4$ standard solution with a $\delta^{34}S$ value of –1.5‰. The Neptune was operated in medium resolution (M/ΔM ~ 8000) to fully resolve oxygen interferences on mass 34. Sample $\delta^{34}S$ reproducibility was typically better than ±0.2‰. Sulfur in residual material, which we refer to as proto-kerogen, was measured as SO_2 by EA-IRMS (Carlo Erba NC 2500 EA connected to a Delta+ XL, ThermoQuest, via the Thermo Conflo III

interface). Proto-kerogen concentrations and $\delta^{34}S$ data have estimated uncertainties based on standard replicates of ± 2.5% and ± 0.5‰, respectively.

2.4 Iron Analyses

A separate aliquot of freeze-dried sediment was weighed and microwave-digested in 16 N reagent-grade HNO_3 (15 min, 1200W) for analysis of total iron (Fe_T) and barium. A 0.5-g aliquot was extracted by the dithionite method to determine 'reducible' iron (Fe_R) primarily in the form of iron (oxy)hydroxides (Raiswell et al., 1994). Sediments (0.5 g) were buffered in 20 mL of 0.35 acetic acid / 0.2 N sodium citrate solution and extracted with 1 g sodium dithionite at room temperature for two hours. Fe_T, Ba and Fe_R were analyzed by inductively coupled plasma optical emission spectrometry (ICP-OES, Perkin-Elmer Optima 7300DV) at the UC Riverside Environmental Sciences Research Laboratory. Uncertainties for Fe_T and Fe_R based on standard replicates are ≤ 2.0%.

2.5 Electron microscopy

To image authigenic pyrite in the Santa Barbara Basin sediments, representative dried sediment samples (from 1, 6, 16, 26, 61, and 215 cm depths) were pressed onto carbon tape, carbon coated, and imaged using a Zeiss 1550VP Field Emission SEM equipped with an Oxford X-Max 80mm^2 SDD EDS system housed at Caltech (12 mm working distance; 120 μm aperture). High-resolution images of the sediment were taken using secondary electron detector and backscatter detector imaging modes to enhance compositional contrast. Energy-dispersive X-ray spectroscopy was used to confirm elemental compositions with accuracy typically better than 5% relative.

3. Results

We discuss our results in terms of three 'zones' representing major features of the dataset. Zone 1 includes the shallowest 10 cm of sediments near the sediment-water interface, and is represented only in multicore data. Zone 2 is present in both the multicore and gravity core between 45 – 55 cm below seafloor, and captures an inflection point in the profiles of some sulfur species. Zone 3 is present only in the gravity core and contains the apparent sulfate-methane transition zone (SMTZ) at 165 – 190 cm depth. Results for the concentration and isotopic composition of dissolved and solid-phase pools are provided in Supplementary Tables 1 and 2, respectively. We compare our multicore and gravity core data with other samples collected in approximately the same area of Santa Barbara Basin, including a box core sample from 2004 (Li et al., 2009) and ODP Hole 893A, which was drilled to 191 m depth (~160,000 yrs) in November 1992 (Bruchert et al., 1995).

Concentration profiles of DIC, sulfate, and sulfide in the gravity core are generally consistent with previously published data (Sholkovitz, 1973; Schimmelmann and Kastner, 1993; Reimers et al., 1996; Kuwabara et al., 1999; Li et al., 2009). These porewater species have distinctly different profiles in the multicores, however, potentially reflecting spatial heterogeneity in the basin. Santa Barbara Basin is characterized by occasional, meter-scale topographic features that could affect sediment accumulation (as observed during Jason ROV operations). Alternatively, the multicore coring site could have been disturbed, either by a recent depositional event or during core collection. To

assess potential disruption at the multicore coring site, we split multicore 'A' in half while still frozen and polished the exposed surface. We observed a distinct, firm, light-toned layer at 5–8 cm within zone 1 that may represent a recent, discrete depositional event associated with a sediment gravity flow. Between 20 and 45 cm depth, the sediment is characterized by mm-scale laminations that are consistent with previous observations (Fleischer, 1972; Soutar and Crill, 1977; Schimmelmann et al., 1990; Schimmelmann and Lange, 1996). Laminations are thicker between 10 and 20 cm and are apparently folded due to subcoring of multicore 'A'. Despite the apparent deformation of these layers, minimally deformed laminae at 8.5 and ~20 cm and substantial gradients of DIC, sulfide, and sulfate across this interval indicate that porewater mixing was not extensive during core collection. In zone 2 and below of multicore 'A', sediments are massive, potentially indicating a period of rapid sedimentation at the multicore sampling site ~100 years ago. Because porewater concentration profiles in the multicore and gravity core may reflect different depositional conditions at each coring site, we did not merge the two cores into a single combined record, but rather discuss them separately in the following discussion.

3.1 Carbon Pools

Total organic carbon (TOC) concentrations, shown in Fig. 2, range from 2.58 to 4.52 mmol C/g dry weight and average 3.29 mmol C/g (4.0 wt.%), with analytical uncertainties of 0.32 mmol C/g. The $\delta^{13}C$ value of this pool averages -22.0‰ and ranges from -22.7 to -21.5‰, with an analytical uncertainty of ±0.1‰. The distributions of TOC values from the gravity core and multicores are comparable in mean and variance, although $\delta^{13}C$ profiles do not match point for point between cores with the current

alignment. In pore water, DIC concentration profiles in the multicore and gravity core (above zone 3) have distinctly different slopes of 0.18 mM/cm and 0.086 mM/cm, respectively. DIC concentrations cease their linear increase in zone 3 and below, where they average 31.4 ± 1.0 mM (1σ). Zone 3 also contains minimum values of DIC $\delta^{13}C$, averaging -24.55 ± 0.45‰ (1σ).

3.2 Iron Pools

Total Fe concentrations in Santa Barbara Basin sediments, shown in Fig. 3, average 307 μmol Fe/g and are similar in both cores. As much as 39% of this Fe is present as reducible iron oxy-hydroxides (ferrihydrite, goethite, lepidocrocite, hematite) near the surface. Dithionite-reducible iron (Fe_R) concentrations average 99.5 ± 2.0 μmol Fe/g in zone 1 (0–10 cm) and decline smoothly to zone 2, where 27.2 μmol Fe_R/g represents only about 10% of total iron. Fe_R concentrations drop more gradually below zone 2, reaching an average of 14.4 μmol Fe/g in zone 3.

3.3 Dissolved Sulfur Pools

Porewater sulfate and sulfide exhibit very different behaviors in the two cores (Fig. 4). In the gravity core, concentrations of sulfate and sulfide are relatively noisy, likely due to the imprecise method of aliquotting porewaters shipboard (analytical standards were much more precise), but nevertheless show roughly linear changes throughout. Sulfate concentrations drop from a maximum concentration of 27.8 mM in the shallowest available sediments to 3.2 mM in zone 3. Over this interval, sulfate becomes increasingly ^{34}S-enriched with a slope of 0.25‰/cm, with a maximum $\delta^{34}S$ value of 61.8‰ at 163 cm.

Standards processed along with sulfate samples from 100 to 160 cm were inaccurate for unknown reasons, and so these data are not reported. Reoxidation of porewater sulfides during squeezer sampling from the gravity core is likely responsible for the convergence of sulfate and sulfide $\delta^{34}S$ values as well as the nonzero sulfate concentrations below zone 3. Accordingly, sulfide concentrations in the gravity core are minimum estimates. Measured sulfide concentrations are near zero (~ 0.05 mM) above 22 cm depth and increase to ~2 mM in zone 3. The sulfur-isotopic composition of this sulfide averages -14‰ in zones 1–2. Below zone 2, sulfide $\delta^{34}S$ increases in parallel with that of sulfate to a maximum value of 22.9‰ at the base of zone 3.

Porewater profiles of sulfate and sulfide in the multicore differ from both the gravity core and previously published profiles (Reimers et al., 1996; Kuwabara et al., 1999) from the Santa Barbara Basin. Below zone 1, sulfate concentrations in the multicore are steadily 22.5 ± 1.9 mM (1σ). Sulfate $\delta^{34}S$ values increase with depth gradually, with a slope of only 0.13‰/cm. In a closed (i.e., Rayleigh-type) system, this change would be equivalent to less than 0.5% consumption of the porewater sulfate reservoir by a reaction with a fractionation factor similar to the offset between porewater sulfate and sulfide at this depth (~30‰). Another surprising difference between the multicore and prior work is the presence of 1.3 mM sulfide in porewater near the sediment-water interface. Below zone 1 in the multicore, the concentration of porewater sulfide is relatively constant at 0.66 ± 0.11 mM (1σ). Over the same interval, however, sulfide $\delta^{34}S$ values exhibit several shifts with amplitudes of roughly 10‰. Below zone 2, sulfide $\delta^{34}S$ is much less variable and increases linearly toward a value of 20‰ in zone 3.

3.4 Solid Sulfur Pools

Concentrations of the major pools of solid-phase sulfur in Santa Barbara Basin sediments are shown in Fig. 5. In general, the concentration and $\delta^{34}S$ profiles of these solid-phase pools are consistent between the multicore and gravity core for the current alignment. Near the sediment-water interface, the pyrite sulfur (S_{py}) pool is slightly larger than the proto-kerogen S (OS_{pk}) pool while the pool of elemental sulfur (S^0) is about half as large. The $\delta^{34}S$ profiles of all three solid sulfur pools share some features, including $\delta^{34}S$ minima within zone 2 and higher $\delta^{34}S$ values in zone 3.

Pyrite concentrations increase with depth from an average of 84 μmol S/g (zone 1) to approximately 135 μmol/g in the deeper multicore or 170 μmol/g in zone 2 of the gravity core. Below zone 2, pyrite concentrations are broadly constant except for a shift toward lower concentrations near the SMTZ (zone 3). Pyrite concentrations in the gravity core average 146 ± 35 μmol S/g between zones 2 and 3 and only 119 ± 15 μmol S/g in zone 3 and below. The isotopic composition of pyrite varies from –20.9 to –38.2‰ and shows complex variation with depth. Pyrite $\delta^{34}S$ values in the multicore decrease dramatically between zones 1 and 2 and have a second minimum at the top of zone 3 in the gravity core.

The highest S^0 concentrations are near the sediment-water interface (zone 1), where they reach 38 ± 4 μmol/g. They decline with depth over the multicore to 5.0 ± 0.5 μmol/g in zone 2. S^0 concentrations in the gravity core also decline with depth, from 2.3 μmol/g in

zone 2 to 0.8 ± 0.1 μmol/g in zone 3. The small amounts of S^0 in deeper sediments have sulfur isotopic compositions that become increasingly ^{34}S-enriched with depth, approaching the composition of dissolved sulfide.

Proto-kerogen S concentrations in the multicore are consistent with depth, averaging 74.5 ± 11.3 μmol/g. This value excludes one extremely OS-rich sample at 6 cm depth containing 156.4 ± 4 μmol/g. In contrast, the gravity core has a depth trend in proto-kerogen S, increasing from a multi-core-like concentration in zone 2 to an average concentration of 89.9 ± 4.1 μmol/g in zone 3. A linear regression of this data yields a slope of approximately 0.12 μmol S/g/cm (R^2 = 0.52). Paired with a less significant decrease in TOC of –2.2 μmol/g/cm (R^2 = 0.13), the molar S:C ratio of proto-kerogen increases from about 1.8% to 3.2% between zones 2 and 3 of the gravity core. Minimum $\delta^{34}S$ values for proto-kerogen S are found in zone 2, where they average –18.8 ± 1.1‰ (1σ). Proto-kerogen $\delta^{34}S$ values increase with depth to an average of –9.3‰ ± 0.9‰ in zone 3. In both cores, proto-kerogen $\delta^{34}S$ values are consistently around 15-20‰ more ^{34}S-enriched than those of coexisting pyrite. The size of this offset is not correlated with solid phase $\delta^{34}S$ values, TOC, or proto-kerogen S:C ratio.

4. Discussion

4.1 Apparent rates of microbial sulfate reduction (MSR)

A fundamental control on the sedimentary sulfur cycle is the rate of microbial sulfate reduction (MSR), which generates the reduced sulfur required for organic S and pyrite formation as well as sulfide-oxidizing metabolisms. Gross rates of MSR may

significantly exceed net rates because microbial communities commonly reoxidize the majority of sulfide produced by MSR (Jorgensen, 1979; Walker and Brimblecombe, 1985; Zerkle et al., 2009). MSR rates have been reported previously for Santa Barbara Basin based on experiments using $^{35}SO_4$ (Reimers et al., 1996), which yielded estimates of 2 to 10 mM/yr in the upper 10 cm and approximately 0.4 mM/yr below ~22 cm depth. In the following section, we constrain the rates of net and gross MSR in our cores based on changes in the abundance and isotopic composition of sedimentary sulfur pools, reducible iron (Fe_R), and DIC. This analysis yields MSR rates that are comparable with those of Reimers et al. in the upper 10 cm but slower in deeper sediments. We convert sediment depths to approximate ages using an age model based on density profiles and varve counts from Schimmelmann et al. (1990; 2013) and visual observation of laminae in multicore 'A.'

Sediments in zone 1 (0–10 cm) show evidence for extensive MSR. Our shallowest porewater sample (0–2 cm) contains substantially more abundant and more ^{13}C-depleted DIC (4.1 mM, -10.7‰) than seawater (2.2 mM, ~0‰), indicating extensive remineralization of organic matter. Due to low concentrations of O_2 in Santa Barbara Basin bottom waters (<10 µM, (Sholkovitz, 1973; Moffitt et al., 2015)), we attribute the majority of this DIC to the respiration of organic carbon by MSR with potential smaller contributions from anaerobic heterotrophy using nitrate, iron, or manganese (porewater nitrate concentrations are <80µM, (Reimers et al., 1996)) and fermentation. Surface sediments also contain 228 ± 23 µmol/g solid-phase reduced sulfur, including pyrite, proto-kerogen, polar extractable OS, and S^0. Each of these phases can act as 'traps' for

the $\sum H_2S$ produced by MSR. If delivery from the water column is assumed to be negligible and zone 1 sediments contain an average of 82 wt% water, this concentration of reduced S solids would represent a sink of approximately 2.6 mmol S/cm^3/yr, equivalent to 3.1 mM/yr dissolved $\sum H_2S$. This rate estimate neglects any $\sum H_2S$ that diffuses out of the sediments or is reoxidized to sulfate. It is not possible to assign strict limits on the extent of sulfide reoxidation to sulfate near the sediment-water interface without data for bottom water O_2 and nitrate concentrations. However, the net rate of solid-phase S change is a minimum estimate of the gross rate of $\sum H_2S$ production. Estimates of minimum MSR rates in zone 1 (at the multicore site) of >2.6 mM/yr are consistent with prior estimates of 2 to 10 mM/yr (Reimers et al., 1996).

Below zone 1, sulfate in porewater reflects the balance of MSR, the reoxidation of reduced S species to sulfate, and net downward diffusion. Neither the multicore nor the gravity core sulfate concentration profiles have any discernable curvature. This is consistent with either an entirely diffusion-controlled regime in which net MSR rates are near zero in sediments between zones 1 and 3 (the SMTZ) or highly efficient sulfur cycling (i.e., MSR followed by complete reoxidation of sulfide back to sulfate). In the absence of O_2, sulfide oxidation may be coupled to the reduction of ferric iron, manganese oxides, or nitrate. Nitrate concentrations were observed to drop toward zero within a few cm of the surface throughout the Santa Barbara Basin (Reimers et al., 1996), so Fe(III)-bearing phases likely represent the primary electron acceptors for sulfide reoxidation below zone 1. The pool we quantify as Fe_R is functionally defined to include easily reducible iron species that have been shown to react with sulfide on a timescale of

hours to days. The Fe in silicates, which makes up the majority of our Fe_T pool, is thought to have a half life of hundreds to tens of thousands of years in reaction with sulfide (Canfield et al., 1992; Raiswell and Canfield, 1998). Therefore, we assume that Fe_R is the most significant electron acceptor below zone 1 in Santa Barbara Basin sediments.

In the multicore, Fe_R concentrations drop from 99.5 μmol/g (18 μmol/cm^3) in zone 1 to 32.3 μmol/g (8.4 μmol/cm^3) in zone 2. Fe_R loss at a rate of 80 nmol/cm^3/yr is balanced by the accumulation of Fe in pyrite, and we tuned the shallow age model to equate these values. Full oxidation of sulfide to sulfate requires the transfer of eight electrons, or eight equivalents of Fe^{3+} reduction. If $\sum H_2S$ is fully oxidized to sulfate, Fe_R loss between zones 1 and 2 is therefore capable of powering the stoichiometric oxidation of $\sum H_2S$ at a rate of 10 nmol/cm^3/yr, equivalent to approximately 13 μM/yr of dissolved $\sum H_2S$ assuming sediment contains 77 wt% water. Partial oxidation of $\sum H_2S$ (e.g., to S^0) could also consume Fe_R without regenerating sulfate, although there is little evidence for S^0 formation below zone 1. Active turnover of the shrinking S^0 pool might be expected to make S^0 $\delta^{34}S$ values more similar to that of actively forming pyrite, while instead we observe S^0 $\delta^{34}S$ values are steady through this interval. The primary biogeochemical role of S^0 in multicore sediments is more likely as a metabolic substrate, as it is lost at a rate of 42 nmol/cm^3/yr.

Based on the availability of oxidants, the rates of MSR in multicore sediments are quite low in sediments below zone 1 (on the order of 0.01 mM/yr). In the gravity core, the abundance of Fe_R declines at an even slower rate (10 nmol/cm^3/yr) and can only account

for the oxidation of around 1 μM/yr of sulfide to sulfate. These rates are several orders of magnitude slower than the several-mM/yr rates implied in zone 1. The linear sulfate concentration profiles in these sediments thus appear to reflect very low MSR rates and a diffusive flux of sulfate down toward the SMTZ (zone 3). Linear DIC profiles are also consistent with a diffusion-controlled porewater regime. The low MSR rates we infer would not generate any observable curvature in the DIC concentration profile, as DIC will diffuse upward from the SMTZ (assuming a diffusion constant of ~1 x 10^{-5} cm^2/sec) at approximately 45 μmol/cm^2/yr.

Low MSR rates between zones 1 and 3 are surprising given the availability of sulfate in pore fluids. MSR in this environment is apparently limited by the availability of electron donors (H_2 or OM) or nutrients (e.g., iron, Sim et al., 2012) rather than electron acceptor (sulfate). Although OM limitation in the presence of 4 wt.% TOC may appear paradoxical, it may instead speak to the importance of OM stabilization near the sediment-water interface. Throughout both cores, OM contains an average of 6.4 wt.% S (molar S:C ratio of 2.4%). We speculate that this S-rich proto-kerogen material may be substantially more resistant to microbial hydrolysis and thus indigestible to heterotrophic sulfate reducers, limiting their growth. Alternatively, sulfate reducers may simply be outcompeted by fermentative organisms that are better at consuming polymeric organic matter.

4.2 Pyrite Formation in Santa Barbara Basin

Pyrite in Santa Barbara Basin sediments appears to form most rapidly near the sediment-water interface, where it is present at an average concentration of 84 μmol S/g. In zone 1, which is only captured in the multi-core, pyrite concentrations are equivalent to ~55% of the concentrations in zone 2. Pyrite $\delta^{34}S$ values in surface sediments are very similar to those of S^0, suggesting that pyrite and S^0 are either genetically related or equilibrate with one another *in situ*. Although rates of pyrite accumulation drop below zone 1, pyrite formation appears to remain an important sink for both sulfur and Fe_R until the base of zone 2, at least in the multi-core. Over this interval, the $\delta^{34}S$ value of pyrite shifts from -25.7‰ to -37.7‰ while porewater $\sum H_2S$ $\delta^{34}S$ values are substantially higher, ranging from 5.9‰ to –19.5‰ (± 0.2‰, Fig 6). In the shallowest sediment sample, the difference between pyrite and $\sum H_2S$ $\delta^{34}S$ values is more than 30‰. Porewater $\sum H_2S$ remains more ^{34}S-enriched than pyrite throughout the gravity core (Fig. 7). Assuming the precipitation process generates small to zero fractionation from its sulfur source (Wilkin and Barnes, 1996; Bottcher et al., 1998), the S-isotopic composition of pyrite cannot be inherited directly from that of porewater $\sum H_2S$ as measured.

Similar isotopic relationships between porewater sulfide and sedimentary pyrite are common in the literature. Kaplan et al (1963), working on shallow (<4 m) sediments from the California Borderland Basins, recorded pyrite that was an average of 24‰ depleted in ^{34}S relative to porewater "free sulfide" and 10‰ depleted relative to "acid volatile sulfide" (AVS). Canfield et al (1992) reported a ^{34}S depletion of fine-grained pyrite relative to porewater "H_2S" of 5-15‰ over 2.5 m of sediment core from Long Island Sound (the FOAM site). Similarly, pyrite was ≥10‰ more ^{34}S-depleted than porewater

sulfide in sediments from Cape Lookout Bight (Chanton and Martens, 1987). Bruchert et al (1996) reported 10-40‰ depletions of pyrite relative to AVS over the nearly 200 m of core from ODP Hole 893A, Santa Barbara Basin. In shallow sediments of St. Andrew's Bay, Florida, Bruchert and Pratt (1996) measured $\delta^{34}S$ values for pyrite that were 0-3‰ more negative than those of $\sum H_2S$, one of the few examples of similar $\delta^{34}S$ values for pyrite and sulfide. Canfield et al (1998) reported a 12-15‰ depletion of "chromium reducible sulfur" (presumed to be mainly pyrite) relative to AVS over 50 cm in Mangrove Lake, Bermuda. Habicht and Canfield (2001) studied shallow (0 – 20 cm) sediments from seven different coastal environments, and obtained direct measurements of sulfide produced by MSR via incubation experiments. The sulfide $\delta^{34}S$ values were uniformly more positive than those of coexisting pyrite, by 5–30‰. In Cariaco Basin, Werne et al (2003) measured pyrite $\delta^{34}S$ values that were 3-5‰ more negative than coeval H_2S, although here the relationship is complicated by water column precipitation of pyrite. Dale et al (2009) studied the upper 5 m of sediment from the Namibian Margin, and found pyrite $\delta^{34}S$ values that are similar to those of porewater H_2S, but in an environment of intense sulfide re-oxidation.

The pattern of ^{34}S-depleted pyrite relative to porewater $\sum H_2S$ that we observe in Santa Barbara Basin thus appears to be common in anoxic marine sediments. Such a pattern is conventionally interpreted as evidence for sulfide oxidation to elemental S, which has a minimal isotope effect, coupled to sulfur disproportionation, which generates sulfide that is 5–16‰ further ^{34}S-depleted and precipitates as pyrite (e.g. Canfield and Thamdrup, 1994; Habicht and Canfield, 2001). A limitation of this hypothesis is the necessity of

somehow separating, in time or space, the sulfide produced by MSR from that produced by sulfur disproportionation. If they mixed prior to forming pyrite, then measurements of porewater $\sum H_2S$ should reveal an isotopic composition similar to pyrite.

Our new dataset from Santa Barbara Basin presents several difficulties for this conventional explanation. First, pyrite and S^0 have similar $\delta^{34}S$ values while porewater sulfide is 33‰ heavier than either solid-phase S pool. Thus S^0 at the sediment surface does not appear to be a direct product of porewater sulfide oxidation, and may instead have the same source as pyrite. Moreover, the disproportionation of S^0 produces fractionations >5‰ (Fry et al., 1986; Canfield, 2001) rather than the <1‰ difference from pyrite we observe in surface sediments. Disproportionation does not therefore appear to play a significant role in controlling pyrite $\delta^{34}S$ in Santa Barbara Basin surface sediments. Last but not least, the high spatial and temporal resolution of our dataset reveals that at no point does the $\delta^{34}S$ value of porewater $\sum H_2S$ approach that of pyrite, eliminating precipitation at shallower levels as a viable explanation.

As an alternative to disproportionation to explain the offset between porewater sulfide and pyrite $\delta^{34}S$, we propose the following hypothesis: the porewater $\sum H_2S$ that we sample is ^{34}S-enriched relative to that produced by MSR, which forms pyrite. The ^{34}S-depleted sulfide generated by MSR could be segregated from bulk porewater sulfide within biological structures like cells (and their sheaths), microbial aggregates, or biofilms. The ε_{MSR} values of $\leq$ 80‰ that are implied by the $\delta^{34}S$ difference between porewater sulfate and accumulating pyrite in Santa Barbara Basin sediments are high but

within known limits (Brunner and Bernasconi, 2005) and are similar to some values reported for ε_{MSR} at low sulfate reduction rates (Canfield et al., 2010; Sim et al., 2011).

Sulfur-cycling biofilms and aggregates are favorable locations for pyrite mineralization because they can both act as sources of $\sum H_2S$ and enhance rates of iron sulfide formation by several orders of magnitude (Frankel and Bazylinski, 2003). Biologically induced mineralization is increasingly seen as having an important role in the precipitation of various iron sulfide minerals, including pyrite (Canfield et al., 1998), pyrrhotite, mackinawite, and greigite (Neal et al., 2001; Schoonen, 2004), although the significance of biologically induced pyrite formation in marine sediments remains essentially unknown. Cell membrane surfaces promote reactions between the FeS* intermediate and S_n^{-2} because their negatively charged surfaces bind metal cations like Fe^{2+} and then stabilize the monosulfide intermediate, promoting crystal nucleation. Pyrite mineralization has been observed in association with enrichment cultures of both sulfur disproportionating and sulfate reducing bacteria. The marine S-disproportionating bacteria *Desulfocapsa* can induce rapid pyrite formation (Canfield et al., 1998) and the sulfate-reducing firmicute *Desulfotomaculum* is capable of mineralizing a bilayer of pyrite on the inside and outside of its cell membrane (Donald and Southam, 1999). Both organisms produce intracellular sulfide that equilibrates in natural systems to form both S_n^{-2} and S^{2-} (Rickard and Luther, 2007). Additionally, many sulfur cycling microorganisms accumulate solid elemental S^0 (Frigaard and Dahl, 2009), which promotes the formation of reactive polysulfide species. Thus, many sulfur-cycling

microorganisms provide a particularly favorable environment for biologically induced pyrite mineralization.

Direct inspection of pyrite grains supports the hypothesis of biologically induced pyrite mineralization in Santa Barbara Basin sediments. Sediment from seven depths were investigated by scanning electron microscopy (SEM), using high backscatter (QBSD) and elemental analysis by energy dispersive spectroscopy (EDS) to image and identify pyrite. At all depths, pyrite phases are exclusively present as sub-micron (~0.3 μm) equidimensional and equimorphic crystals, often aggregated into framboids. Examples are shown in Fig. 8. Although pyrite framboids have been shown to form abiotically at elevated temperatures (60 to 350° C) (MacLean et al., 2008), no laboratory studies have yet generated framboids abiotically at lower temperatures (Ohfuji and Rickard, 2005). Recent work by MacLean et al. (2008) provides evidence for the formation of framboidal pyrite on organic templates within microbial biofilms (Wacey et al., 2014). The pyrites observed in Santa Barbara Basin sediments are therefore consistent with biologically induced pyrite mineralization in association with sulfate-reducing microbial communities. We propose that the highly ^{34}S-depleted sulfide produced by MSR reacts to form pyrite within relatively isolated microbial biofilm environments and that the $\sum H_2S$ that diffuses away from this environment into porewater can subsequently become more ^{34}S-enriched via additional processes (discussed below). A key aspect of this hypothesis is that it can account for S^0 with $\delta^{34}S$ values similar to pyrite. We further note that generation of ^{34}S-depleted sulfide by MSR and sulfur disproportionation are not mutually exclusive, and both could contribute to pyrite formation.

4.3 Potential controls on porewater sulfide $\delta^{34}S$

What additional processes might explain the consistent ^{34}S-enrichment of porewater sulfide relative to pyrite, proto-kerogen S, and S^0? We propose that isotopic exchange with organic sulfur is a prime candidate. Porewater $\sum H_2S$ and proto-kerogen have very similar $\delta^{34}S$ values in the upper 35 cm of the gravity core (within ~2‰). Below this depth, $\sum H_2S$ $\delta^{34}S$ values increase approximately linearly (Fig. 7), likely reflecting the upward flux of $\sum H_2S$ produced near the SMTZ (zone 3). The S-isotope composition of proto-kerogen partially follows that of porewater $\sum H_2S$ throughout deeper sediments and into the ODP core. In the presence of low MSR rates, these patterns suggest isotopic equilibration between these pools, especially in the upper part of the core. In Santa Barbara Basin, equilibration can drive particularly large $\delta^{34}S$ offsets between pyrite and proto-kerogen because proto-kerogen S is highly abundant while rates of $\sum H_2S$ production are low. Therefore, the equilibrium $\delta^{34}S$ value of the $\sum H_2S$ + OS system should be dominated by the proto-kerogen pool rather than by $\sum H_2S$. In environments with higher MSR rates and less abundant proto-kerogen S, equilibration would lead to smaller offsets between pyrite and proto-kerogen. In either case, phases precipitating within MSR-hosting microenvironments (e.g., pyrite) should trap the most strongly ^{34}S-depleted $\sum H_2S$, while $\sum H_2S$ that diffuses out of microenvironments into porewater can undergo isotopic exchange with abundant, ^{34}S-enriched organic matter and become more ^{34}S-enriched.

Dale et al. (2009) found similar evidence for equilibration between porewater $\sum H_2S$ and proto-kerogen in Namibian shelf sediments, where TOC and proto-kerogen S concentrations are comparable to those in Santa Barbara Basin. Their model suggested that ~70% of proto-kerogen S and a similar proportion of S_{py} were exchangeable. However, with nearly 18 mM porewater $\sum H_2S$ (130 cm depth), isotopic equilibration between porewater $\sum H_2S$ and some proto-kerogen S in Namibian shelf sediments has a strong effect on the $\delta^{34}S$ value of the organic matter but a negligible effect on porewater $\sum H_2S$ (Dale et al., 2009), which is the opposite situation from Santa Barbara Basin. Also unlike that study, we find no evidence for isotopic exchange between porewater sulfide and pyrite in our samples. This difference may reflect different conditions of pyrite formation in Santa Barbara Basin and the Namibian Shelf, where rates of sulfate reduction are much higher and pyrite formation occurs deeper in the sediments.

Even more so than for proto-kerogen, polar extractable OS $\delta^{34}S$ values track $\sum H_2S$ $\delta^{34}S$ in the shallow multicore. Both the extractable OS and porewater $\sum H_2S$ multicore $\delta^{34}S$ profiles reproduce a sharp shift from values near -10‰ at 10 cm depth to around 0‰ at 20 cm. Equilibration between OS and porewater sulfide is a potential mechanism to maintain this strong of an isotopic gradient despite ongoing diffusion. Although the quantity of sulfur in polar extractable OS alone is insufficient to control the $\delta^{34}S$ value of porewater sulfide, polar extractable OS may be representative of the portion of proto-kerogen S that is exchangeable. Essentially, we propose that sulfide $\delta^{34}S$ values in shallow sediments are buffered by local exchange with OS, including polar extractable OS and part of the larger proto-kerogen pool. In this interpretation, the large (~10‰)

shifts in the shallow multicore porewater $\sum H_2S$ profile represent a primary depositional signal in exchangeable OS $\delta^{34}S$, likely controlled by the sediment gravity flow recorded at 5–8 cm depth. These sediments are also characterized by peak concentrations of FeR, TOC, and proto-kerogen OS and relatively ^{34}S-enriched pyrite and S^0.

Porewater sulfide $\delta^{34}S$ could also be influenced by fractionations associated with metabolic sulfide oxidation. For example, porewater $\sum H_2S$ $\delta^{34}S$ values are 4.3‰ more ^{34}S-enriched than even polar extractable OS in the shallowest multicore sample, which could result from the preferential reoxidation of ^{32}S by sulfide oxidizing microorganisms. Sulfide oxidation coupled to O_2 is associated with a fractionation factor of about –5.2‰ (Fry et al., 1988), while sulfide oxidation coupled to nitrate reduction imparts a similar fractionation of –1.3 to –4.3‰ (Poser et al., 2014). In either case, sulfide oxidation is therefore expected to leave the residual sulfide pool relatively ^{34}S-enriched, which is the pattern we observe in the shallowest 5 cm of the multicore. Given the complicating factors of diffusion, exchange, variable bottom water oxidant concentrations, and a potential flood layer in the shallowest part of the multicore, we cannot estimate rates of sulfide oxidation in zone 1 with certainty. Regardless, if we assume that porewater $\sum H_2S$ has an 'initial' $\delta^{34}S$ value matching extractable OS and is removed only by oxidation with a fractionation factor of -1.3 or –4.3‰, the approximately 5‰ enrichment we observe in our shallowest multicore sample could be achieved by reoxidation of approximately 98% or 69%, respectively, of the $\sum H_2S$ pool. Below zone 1, sulfide oxidation is likely oxidant-limited and constrained to low rates by Fe_R concentration data (Section 4.1).

4.4 The generation of sedimentary sulfur isotope records

Pyrite $\delta^{34}S$ values are often interpreted in terms of their formation under idealized closed-system or open-system conditions, following Jorgensen (1979). In the first case, $\sum H_2S$ is diffusion-limited and pyrite $\delta^{34}S$ values reflect progressive distillation of the $\sum H_2S$ reservoir, generating relatively heterogeneous and ^{34}S-enriched pyrite (e.g., Gautier, 1986). In the open-system case, $\sum H_2S$ can be thought of as an infinite reservoir, and pyrite forms with a relatively low and invariant isotopic composition (e.g., Lyons, 2003). Sedimentary environments like central Santa Barbara Basin are particularly poorly suited to these idealized models because the chemocline is located near the sediment-water interface, where the local environments hosting pyrite precipitation may be fairly restricted while dissolved species are strongly affected by diffusive and advective processes. Pyrite $\delta^{34}S$ values in this environment may be particularly sensitive to secular changes in the precise position of the chemocline, which is likely to respond dynamically to changes in bottom water chemistry and sediment supply. If the deep water column becomes sufficiently suboxic (e.g., Ploug, 2001), it is possible that large particles could host MSR and act as an episodic source of pyrite or abiogenic OS to surface sediments. Additionally, changes in the O_2 content of bottom waters or fluxes of labile organic matter could affect the rate of MSR and by extension, its fractionation factor and the $\delta^{34}S$ value of the $\sum H_2S$ recorded as pyrite.

The pyrite and organic S generated in shallow sediments represent potential archives of information about depositional conditions and biogeochemical cycling, with the usual caveat regarding the extent to which their $\delta^{34}S$ values are preserved during later sediment

diagenesis. Pyrite $\delta^{34}S$ values from our shallow cores as well as ODP Hole 893A appear to reflect temporal variability in sediment deposition and redox conditions. Both profiles have no simple trends with depth and share a $\delta^{34}S$ range of -39.0 to -15.4‰ (Figs. 6 and 7, Bruchert et al., 1995). Proto-kerogen $\delta^{34}S$ profiles are smoother and Hole 893A data are less variable, reflecting the influence of S exchange with other pools. However, this exchange does not continue indefinitely. Outside of zone 1, polar extractable OS $\delta^{34}S$ values from the multi-, gravity, and box cores are remarkably consistent with Hole 893A (Bruchert et al., 1995), suggesting that equilibration between polar extractable OS and $\sum H_2S$ does not continue below surface sediments. Moreover, porewater $\sum H_2S$ and proto-kerogen $\delta^{34}S$ values diverge below zone 2 in the gravity core, suggesting that proto-kerogen becomes more stable and resistant to exchange at this point in the diagenetic sequence. Nevertheless, some amount of OS apparently continues to exchange below the SMTZ, because proto-kerogen in ODP Hole 893A is more ^{34}S-enriched than any proto-kerogen in our core (Figs. 6 and 7). Diagenetic reactions may change the dominant type of S-bearing organic matter structure over time and reduce the exchangeability of OS, for example as thiol groups convert to more stable sulfides, thiophenes, and/or polysulfide bridges (Kohnen et al., 1989; Damsté and De Leeuw, 1990; Vairavamurthy et al., 1994). Proto-kerogen $\delta^{34}S$ values will be affected by exchange processes and biogeochemical sulfur cycling as long as a significant proportion of OS remains exchangeable.

The $\delta^{34}S$ difference between proto-kerogen and pyrite may contain useful information for reconstructing paleoenvironments. In our hypothesis, the degree of ^{34}S enrichment of OS relative to pyrite should be related to the relative abundances of OS versus $\sum H_2S$. At sites

with high rates of MSR, OS should be more similar to locally forming pyrite because abundant porewater $\sum H_2S$ dominates the exchangeable sulfur reservoir. In contrast, if the flux of $\sum H_2S$ to porewater is relatively low, we predict OS should retain a more ^{34}S-enriched composition reflecting the influence of biosulfur. In Santa Barbara Basin, the location of the chemocline at the sediment-water interface encourages the formation of abundant OS that appears to survive with minimal degradation over the next several hundred years, potentially limiting MSR. This environment is particularly conducive to $\sum H_2S$ – OS exchange and generates a relatively large (>15‰) $\delta^{34}S$ difference between coexisting pyrite and proto-kerogen. Further work is clearly warranted to help us interpret records of pyrite and OS $\delta^{34}S$ as well as their difference in naturally dynamic sedimentary environments.

5. Conclusions

Pyrite formation is a complex process that occurs at the intersection of multiple microbial metabolisms, abiotic reactions, and physical processes in sediments. We studied the distribution of ^{34}S among all the major dissolved and solid sulfur species to constrain the pathways of pyrite formation in Santa Barbara Basin. Consistent with previous work, we find evidence for the accumulation of pyrite with very low $\delta^{34}S$ values of -30 to -40‰ throughout the upper part of the core, where porewater $\sum H_2S$ has $\delta^{34}S$ values ranging from 5.9 to -19.5‰. However, our observation that S^0 has $\delta^{34}S$ values matching those of pyrite, not $\sum H_2S$, largely rules out sulfur disproportionation as a possible reason for this isotopic disparity. From electron microscopy, sub-micron pyrite crystals are very consistent in size and shape, intergrown with amorphous materials, and commonly

agglomerated into framboids—morphologies that are consistent with pyrite forming in association with organic structures, cell walls and biofilms. We therefore propose that pyrite is the product of the sulfide generated by microbial sulfate reduction (MSR) within biofilms or aggregates. In Santa Barbara Basin, only a small flux of $\sum H_2S$ then diffuses into porewater, where it is exposed to a relatively large pool of organic sulfur (OS) that is at least partially exchangeable. Sulfur isotopic exchange between porewater $\sum H_2S$ and OS would tend to enrich the smaller $\sum H_2S$ pool in ^{34}S, potentially explaining the isotopic composition of these pools in our shallow core (zones 1 and 2). In deeper sediments, porewater $\sum H_2S$ and other dissolved species appear to be controlled primarily by diffusion related to processes at the SMTZ (zone 3) at ~165–190 cm depth.

These results illustrate the complexity of the sulfur cycle in organic-rich marine sediments and support a significant role for microbially-driven microenvironments in pyrite formation. Despite this complexity, if pyrite is indeed recording the isotopic composition of the $\sum H_2S$ produced by MSR, it can represent a relatively straightforward and potentially powerful archive of paleoenvironmental information. Complementary information about the relative abundance of $\sum H_2S$ and OS can also be recorded in the $\delta^{34}S$ difference between OS and pyrite in marine sediments.

Acknowledgements

We gratefully acknowledge the science team and crew of *R/V Atlantis* cruise AT26-06, especially the efforts of Katherine S Dawson (Caltech), David L. Valentine, Karin

Lemkau, and Alex Phillips (UC Santa Barbara). This work benefitted from helpful discussions with Victoria J. Orphan and Guillaume Paris, analytical support from David Lyons (UC Riverside) and Fenfang Wu (Caltech), and assistance with sediment extractions from Emilia S. Hernandez. Funding was provided by the National Science Foundation award OCE1436566 to A.L.S. and the Gordon and Betty Moore Foundation through Grant GBMF#3306 to A.L.S.. This manuscript was much improved by insightful reviews from David Fike (Washington U. in St. Louis), Maya Gomes (Harvard), and Matt Hurtgen (Northwestern U.) and the careful editorial handling of Claire Rollion-Bard.

References

Anderson T. F. and Pratt L. M. (1995) Isotopic evidence for the origin of organic sulfur and elemental sulfur in marine sediments. *ACS Symposium Series* **612**, 378–396.

Berelson W. M., Prokopenko M., Sansone F. J., Graham A. W., McManus J. and Bernhard J. M. (2005) Anaerobic diagenesis of silica and carbon in continental margin sediments: Discrete zones of TCO_2 production. *Geochimica et Cosmochimica Acta* **69**, 4611–4629.

Berner R. A. and Raiswell R. (1983) Burial of organic carbon and pyrite sulfur in sediments over Phanerozoic time: a new theory. *Geochimica et Cosmochimica Acta* **47**, 855–862.

Bontognali T. R., Sessions A. L., Allwood A. C., Fischer W. W., Grotzinger J. P., Summons R. E., Eiler J. M. (2012) Sulfur isotopes of organic matter preserved in 3.45-billion-year-old stromatolites reveal microbial metabolism. *Proceedings of the National Academy of Sciences* **109**, 15146–15151.

Bottcher M., Smock A. and Cypionka H. (1998) Sulfur isotope fractionation during experimental precipitation of iron(II) and manganese(II) sulfide at room temperature. *Chemical Geology* **146**, 127–134.

Bottrell S. and Newton R. (2006) Reconstruction of changes in global sulfur cycling form marine sulfate isotopes. *Earth Science Reviews* **75**, 59–83.

Bottrell S. H. and Raiswell R. (2000) Sulphur isotopes and microbial sulphur cycling in sediments. In *Microbial Sediments*, eds. Riding R. E. and Awramik S.M., 96–104.

Bruchert V., Pratt L. M., Anderson T. F. and Hoffmann S. R. (1995) Abundance and isotopic composition of organic and inorganic sulfur species in laminated and bioturbated sediments from Hole 893A, Santa Barbara Basin eds. J. P. Kennett, J. G. Baldauf, and M. Lyle. *Proceedings of the Ocean Drilling Program, Scientific Results* **146**, 219–230.

Brunner B. and Bernasconi S. (2005) A revised isotope fractionation model for dissimilatory sulfate reduction in sulfate reducing bacteria. *Geochimica et Cosmochimica Acta* **69**, 4759–4771.

Butler I. B., Böttcher M. E., Rickard D. and Oldroyd A. (2004) Sulfur isotope partitioning during experimental formation of pyrite via the polysulfide and hydrogen sulfide pathways: implications for the interpretation of sedimentary and hydrothermal pyrite isotope records. *Earth and Planetary Science Letters* **228**, 495–509.

Canfield D. (2004) The evolution of the earth surface sulfur reservoir. *American Journal of Science* **304**, 839–861.

Canfield D. and Teske A. (1996) Late Proterozoic rise in atmospheric oxygen concentration inferred from phylogenetic and sulphur-isotope studies. *Nature* **382**, 127–132.

Canfield D. E. (2001) Biogeochemistry of Sulfur Isotopes. *Reviews in Mineralogy and Geochemistry* **43**, 607–636.

Canfield D. E. and Thamdrup B. (1994) The production of 34S-depleted sulfide during bacterial disproportionation of elemental sulfur. *Science* **266**, 1973.

Canfield D. E., Raiswell R. and Bottrell S. H. (1992) The reactivity of sedimentary iron minerals toward sulfide. *American Journal of Science* **292**, 659–683.

Canfield D. E., Thamdrup B. and Fleischer S. (1998) Isotope fractionation and sulfur metabolism by pure and enrichment cultures of elemental sulfur-disproportionating bacteria. *Limnology and Oceanography* **43**, 253–264.

Canfield D., Farquhar J. and Zerkle A. (2010) High isotope fractionations during sulfate reduction in a low-sulfate euxinic ocean analog. *Geology* **38**, 415–418.

Canfield D., Olesen C. and Cox R. (2006) Temperature and its control of isotope fractionation by a sulfate-reducing bacterium. *Geochimica et Cosmochimica Acta* **70**, 548–561.

Chanton and Martens C. (1987) Biogeochemical cycling in an organic-rich coastal marine basin. 8. A sulfur isotopic budget balanced by differential diffusion across the sediment-water interface. *Geochimica et Cosmochimica Acta* **51**, 1201–1208.

Dale A. W., Bruchert V., Alperin M. and Regnier P. (2009) An integrated sulfur isotope model for Namibian shelf sediments. *Geochimica et Cosmochimica Acta* **73**, 1924–1944.

Damsté J. S. S. and De Leeuw J. W. (1990) Analysis, structure and geochemical significance of organically-bound sulphur in the geosphere: state of the art and future research. *Organic Geochemistry* **16**, 1077–1101.

Detmers J., Bruchert V., Habicht K. and Kuever J. (2001) Diversity of sulfur isotope fractionations by sulfate-reducing prokaryotes. *Applied and Environmental Microbiology* **67**, 888–894.

Donald R. and Southam G. (1999) Low temperature anaerobic bacterial diagenesis of ferrous monosulfide to pyrite. *Geochimica et Cosmochimica Acta* **63**, 2019–2023.

Fleischer P. (1972) Mineralogy and sedimentation history, Santa Barbara Basin, California. *Journal of Sedimentary Petrology* **42**, 49–58.

Frankel R. B. and Bazylinski D. A. (2003) Biologically induced mineralization by bacteria. *Reviews in Mineralogy and Geochemistry* **54**, 95–114.

Frigaard N. U. and Dahl C. (2009) Sulfur metabolism in phototrophic sulfur bacteria. In *Advances in Microbial Physiology*, ed. Poole R. K.. London: Academic Press, 103-200.

Froelich P. N., Klinkhammer G. P., Bender M. L., Luedtke N. A., Heath G. R., Cullen D. and Dauphin P. (1979) Early oxidation of organic matter in pelagic sediments of the eastern equatorial Atlantic: suboxic diagenesis. *Geochimica et Cosmochimica Acta* **43**, 1075–1090.

Fry B., Cox J., Gest H. and Hayes J. M. (1986) Discrimination between ^{34}S and ^{32}S

during bacterial metabolism of inorganic sulfur compounds. *Journal of Bacteriology* **165**, 328–330.

Fry B., Jannasch H. W., Molyneaux S. J., Wirsen C. O., Muramoto J. A. and King S. (1991) Stable isotope studies of the carbon, nitrogen and sulfur cycles in the Black Sea and the Cariaco Trench. *Deep Sea Research Part A, Oceanographic Research Papers* **38**, S1003–S1019.

Fry B., Ruf W., Gest H. and Hayes J. M. (1988) Sulfur isotope effects associated with oxidation of sulfide by O2 in aqueous solution. *Chemical Geology: Isotope Geoscience Section* **73**, 205–210.

Gautier, D. L. (1987). Isotopic composition of pyrite: relationship to organic matter type and iron availability in some North American Cretaceous shales. *Chemical Geology: Isotope Geoscience Section*, **65**, 293–303.

Goldhaber M. B. and Kaplan I. R. (1975) Controls and consequences of sulfate reduction rates in recent marine sediments. *Soil Science* **119**, 42–55.

Habicht K. S. and Canfield D. E. (2001) Isotope fractionation by sulfate-reducing natural populations and the isotopic composition of sulfide in marine sediments. *Geology* **29**, 555–558.

Habicht K., Gade M., Thamdrup B., Berg P. and Canfield D. (2002) Calibration of sulfate levels in the Archean ocean. *Science* **298**, 2372–2374.

Harrison B., Zhang H., Berelson W. and Orphan V. (2009) Variations in archaeal and bacterial diversity associated with the sulfate-methane transition zone in continental margin sediments (Santa Barbara Basin, California). *Applied and Environmental Microbiology* **75**, 1487–1499.

Johnston D., Wing B., Farquhar J., Kaufman A., Strauss H., Lyons T., Kah L. and Canfield D. (2005) Active microbial sulfur disproportionation in the Mesoproterozoic. *Science* **310**, 1477–1479.

Johnston D., Farquhar J., Canfield D. (2007) Sulfur isotope insights into microbial sulfate reduction: When microbes met models. *Geochimica et Cosmochimica Acta* **71**, 3929–3947.

Jorgensen B. B. (1979) A theoretical model of the stable sulfur isotope distribution in marine sediments. *Geochimica et Cosmochimica Acta* **43**, 363–374.

Jorgensen B. B. (1982) Mineralization of organic matter in the sea bed-the role of sulphate reduction. *Nature* **296**, 643–645.

Kaplan I. R. and Rittenberg S. C. (1964) Microbiological fractionation of sulphur isotopes. *Journal of General Microbiology* **34**, 195–212.

Kohnen M., Damste J. S., ten Haven H. L. and De Leeuw J. W. (1989) Early incorporation of polysulfides in sedimentary organic matter. *Nature* **341**, 640–641.

Kuwabara J. S., van Geen A., McCorkle D. C. and Bernhard J. M. (1999) Dissolved sulfide distributions in the water column and sediment pore waters of the Santa Barbara Basin. *Geochimica et Cosmochimica Acta* **63**, 2199–2209.

Leavitt W. D., Halevy I., Bradley A. S. and Johnston D. T. (2013) Influence of sulfate reduction rates on the Phanerozoic sulfur isotope record. *Proceedings of the National Academy of Sciences*.

Li C., Sessions A. L., Kinnaman F. S. and Valentine D. L. (2009) Hydrogen-isotopic variability in lipids from Santa Barbara Basin sediments. *Geochimica et Cosmochimica Acta* **73**, 4803–4823.

MacLean L., Tyliszczak, Gilbert P., Zhou D., Pray T. J., Onstott T. C. and Southam G. (2008) A high-resolution chemical and structural study of framboidal pyrite formed within a low-temperature bacterial biofilm. *Geobiology* **6**, 471–480.

Moffitt S. E., Hill T. M., Ohkushi K., Kennett J. P. and Behl R. J. (2014) Vertical oxygen minimum zone oscillations since 20 ka in Santa Barbara Basin: A benthic foraminiferal community perspective. *Paleoceanography* **29**, 44–57.

Moffitt S. E., Moffitt R. A., Sauthoff W., Davis C. V., Hewett K. and Hill T. M. (2015) Paleoceanographic Insights on Recent Oxygen Minimum Zone Expansion: Lessons for Modern Oceanography ed. Y. Hong. *PLOS ONE* **10**, e0115246.

Neal A. L., Techkarnjanaruk S., Dohnalkova A., McCready D., Peyton B. M. and Geesey G. G. (2001) Iron sulfides and sulfur species produced at hematite surfaces in the presence of sulfate-reducing bacteria. *Geochimica et Cosmochimica Acta* **65**, 223–235.

Ohfuji H. and Rickard D. (2005) Experimental syntheses of framboids—a review. *Earth Science Reviews* **71**, 147–170.

Orphan V. J., Hinrichs K. U., Ussler W., Paull C. K., Taylor L. T., Sylva S. P., Hayes J. M. and Delong E. F. (2001) Comparative Analysis of Methane-Oxidizing Archaea and Sulfate-Reducing Bacteria in Anoxic Marine Sediments. *Applied and Environmental Microbiology* **67**, 1922–1934.

Paris G., Adkins J. F., Sessions A. L. and Subhas A. (2013) MC-ICP-MS measurement of $\delta^{34}S$ and $\Delta^{33}S$ in small amounts of dissolved sulfate. *Chemical Geology* **345**, 50–61.

Poser, A., Vogt, C., Knöller, K., Ahlheim, J., Weiss, H., Kleinsteuber, S., & Richnow, H.-H. (2014). Stable Sulfur and Oxygen Isotope Fractionation of Anoxic Sulfide Oxidation by Two Different Enzymatic Pathways. *Environmental Science and Technology*, **48**, 9094–9102.

Raiswell R. and Canfield D. (1998) Sources of iron for pyrite formaiton in marine sediments. *American Journal of Science* **298**, 219–245.

Raiswell R., Canfield D. E. and Berner R. A. (1994) A comparison of iron extraction methods for the determination of degree of pyritisation and the recognition of iron-limited pyrite formation. *Chemical Geology* **111**, 101–110.

Rees C. E. (1973) A steady-state model for sulphur isotope fractionation in bacterial reduction processes. *Geochimica et Cosmochimica Acta* **37**, 1141–1162.

Reimers C. E., Lange C. B., Tabak M. and Bernhard J. M. (1990) Seasonal spillover and varve formation in the Santa Barbara Basin, California. *Limnology and Oceanography* **35**, 1577–1585.

Reimers C. E., Ruttenberg K. C., Canfield D. E., Christiansen M. B. and Martin J. B. (1996) Porewater pH and authigenic phases formed in the uppermost sediments of the Santa Barbara Basin. *Geochimica et Cosmochimica Acta* **60**, 4037–4057.

Rickard D. and Luther G. I. (2007) Chemistry of Iron Sulfides. *Chemical Reviews* **107**, 514–562.

Rickard, D., & Morse, J. (2005). Acid volatile sulfide (AVS). *Marine Chemistry*, **97**, 141–197.

Schimmelmann A. and Kastner M. (1993) Evolutionary changes over the last 1000 years of reduced sulfur phases and organic carbon in varved sediments of the Santa Barbara Basin, California. *Geochimica et Cosmochimica Acta* **57**, 67–78.

Schimmelmann A. and Lange C. B. (1996) Tales of 1001 varves: a review of Santa Barbara Basin sediment studies. *Geological Society, London, Special Publications* **116**, 121–141.

Schimmelmann A., Hendy I. L., Dunn L., Pak D. K. and Lange C. B. (2013) Revised ~2000-year chronostratigraphy of partially varved marine sediment in Santa Barbara Basin, California. *GFF* **135**, 258–264.

Schimmelmann A., Lange C. B. and Berger W. H. (1990) Climatically controlled marker layers in Santa Barbara Basin sediments and fine-scale core-to-core correlation. *Limnology and Oceanography* **35**, 165–173.

Schoonen M. (2004) Mechanisms of sedimentary pyrite formation eds. J. Amend, K. Edwards, and T. W. Lyons. *GSA Special Papers* **379**, 117–134.

Sholkovitz E. (1973) Interstitial water chemistry of the Santa Barbara Basin sediments. *Geochimica et Cosmochimica Acta* **37**, 2043–2073.

Sim M. S., Bosak T. and Ono S. (2011a) Large sulfur isotope fractionation does not require disproportionation. *Science* **333**, 74–77.

Sim M. S., Ono S., Donovan K., Templer S. P., Bosak T. (2011b) Effect of electron donors on the fractionation of sulfur isotopes by a marine *Desulfovibrio* sp.. *Geochimica et Cosmochimica Acta* **75**, 4244–4259.

Soutar A. and Crill P. A. (1977) Sedimentation and climatic patterns in the Santa Barbara Basin during the 19th and 20th centuries. *Geological Society of America Bulletin* **88**, 1161–1172.

Vairavamurthy A., Zhou W., Eglinton T. and Manowitz B. (1994) Sulfonates: a novel class of organic sulfur compounds in marine sediments. *Geochimica et Cosmochimica Acta* **58**, 4681–4687.

Wacey D., Kilburn M. R., Saunders M., Cliff J. B., Kong C., Liu A. G., Matthews J. J. and Brasier M. D. (2014) Uncovering framboidal pyrite biogenicity using nano-scale CNorg mapping. *Geology* **43**, 27–30.

Walker J. C. G. and Brimblecombe P. (1985) Iron and sulfur in the pre-biologic ocean. *Precambrian Research* **28**, 205 – 222.

Wilkin R. T. and Barnes H. L. (1996) Pyrite formation by reactions of iron monosulfides

with dissolved inorganic and organic sulfur species. *Geochimica et Cosmochimica Acta* **60**, 4167–4179.

Zerkle A., Farquhar J., Johnston D., Cox R. and Canfield D. (2009) Fractionation of multiple sulfur isotopes during phototrophic oxidation of sulfide and elemental sulfur by a green sulfur bacterium. *Geochimica et Cosmochimica Acta* **73**, 291–306.

Figure Captions

Figure 1. Sample analysis workflow (see text for methodological details).

Figure 2: Concentrations and isotopic compositions of total organic carbon (TOC) and dissolved inorganic carbon (DIC). Shaded bands refer to zones (1-3, at right) discussed in text. TOC $\delta^{13}C$ values are repeated in panel D for comparison. Filled symbols represent gravity core results, and open symbols represent multicore results. Lines on TOC plots show three-point running averages. Porewater DIC results for the multi- and gravity cores are shown in light (grey) and darker (orange) lines, respectively. DIC concentration uncertainties are approximately ±2%. Uncertainties for DIC $\delta^{13}C$ data are less than the line width.

Figure 3: Concentrations of iron pools in Santa Barbara Basin sediments. Total iron (Fe_{TOT}), reducible iron (Fe_R), and a running 3-point average of pyrite (Fe_{Py}) iron are shown as circles, triangles, and a thin line, respectively. Fe_{Py} data from the multicore are shown as open squares. Open triangles represent multi-core data; filled triangles are from the gravity core and filled black symbols with vertical error bars are from the box core. Fe_{Py} is calculated from S_{py} results assuming an ideal 2:1 S:Fe stoichiometry. Shaded bands indicate zones discussed in the text. The right panel shows the same Fe_R data as at left but with expanded x-axis for clarity. Error bars for Fe_T and Fe_R are smaller than symbols.

Figure 4: Concentrations and isotopic compositions of sulfate and sulfide in porewater from the multicore (top) and gravity core (bottom). $\delta^{34}S$ values are relative to VCDT, and have analytical uncertainties smaller than symbols. Shaded bands (labeled at right) indicate zones discussed in the text.

Figure 5: Concentrations and isotopic compositions of solid-phase sulfur pools in Santa Barbara Basin sediments, including pyrite (S_{py}), proto-kerogen (OS_{pk}), elemental S (S^0), and polar extractable OS. Shaded bars, labeled at right, indicate zones discussed in the text. Open symbols represent multicore data; filled symbols represent gravity core data, and filled symbols at 5 cm are from the box core. Three-point running averages are shown for gravity core S_{py} and OS_{pk} (black lines) and multicore S_{py} (grey line).

Figure 6: $\delta^{34}S_{VCDT}$ relationships among reduced sulfur pools in multicore sediments and ODP Hole 893A. Solid black symbols at 5 cm depth represent data for the box core. Symbols represent pyrite (S_{py}, squares), elemental S (S^0, open circles), proto-kerogen (OS_{pk}, triangles), porewater sulfide ($\sum H_2S$, red line); polar extractable OS (Xs), and porewater sulfate (SO_4^{2-}, small filled circles). ODP Hole 893A samples were collected between 0.9 and 192 m below sea floor; data from (Bruchert et al., 1995). Grey bands, numbered at right, correspond to zones discussed in the text.

Figure 7: $\delta^{34}S_{VCDT}$ relationships among reduced sulfur pools in gravity core sediments and ODP Hole 893A. Solid black symbols at 5 cm depth represent data for the box core. Symbols represent pyrite (S_{py}, squares), elemental S (S^0, open circles), proto-kerogen (OS_{pk}, triangles), porewater sulfide ($\sum H_2S$, red line); polar extractable OS

(Xs), and porewater sulfate (SO_4^{2-}, small filled circles). ODP Hole 893A samples were collected between 0.9 and 192 m below sea floor; data from (Bruchert et al., 1995).

Figure 8: Secondary electron photomicrographs of authigenic pyrites within siliciclastic Santa Barbara Basin sediments. Samples are stuck on carbon tape and carbon-coated; bright contrast in the foreground of A is due to charging. Phase identifications were confirmed using EDS. A: Cluster of ~10 μm diameter framboidal pyrites (26 cm sample); B: Individual pyrite crystals within an amorphous matrix (26 cm sample); C: Typical framboid morphology (215 cm sample).

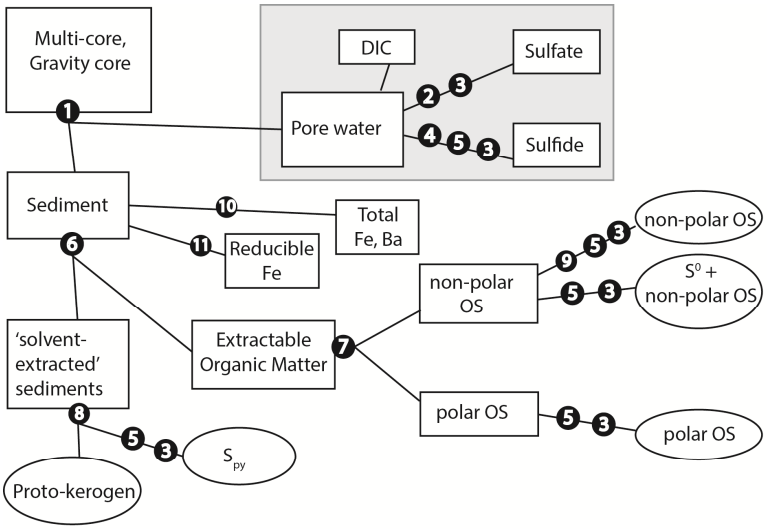

1. Squeeze or rhizon sample cores
2. Acidification
3. Anion exchange chromatography
4. Trap sulfide with zinc acetate
5. Oxidation by H_2O_2 at 90°C
6. Microwave extraction in organic solvent
7. Silica gel chromatography
8. 1N HNO_3 leach, 12 days
9. Cu treatment
10. Microwave digestion in 16N HNO_3
11. Sodium dithionite extraction